PHILOSOPHICAL TRANSACTIONS OF THE ROYAL SOCIETY A MATHEMATICAL, PHYSICAL & ENGINEERING SCIENCES

Basin Explosions and Escape Phenomena in the Twin-Well Duffing Oscillator: Compound Global Bifurcations Organizing Behaviour

Y. Ueda, S. Yoshida, H. B. Stewart and J. M. T. Thompson

Phil. Trans. R. Soc. Lond. A 1990 **332**, 169-186
doi: 10.1098/rsta.1990.0107

Basin explosions and escape phenomena in the twin-well Duffing oscillator: compound global bifurcations organizing behaviour

By Y. Ueda[1], S. Yoshida, H. B. Stewart[2] and J. M. T. Thompson[3]

[1] *Department of Electrical Engineering, Kyoto University, Kyoto, Japan*
[2] *Mathematical Sciences Division, Brookhaven National Laboratory, Upton, New York 11973, U.S.A.*
[3] *Department of Civil Engineering, University College London, Gower Street, London WC1E 6BT, U.K.*

The sinusoidally drive, twin-well Duffing oscillator has become a central archetypal model for studies of chaos and fractal basin boundaries in the nonlinear dynamics of dissipative ordinary differential equations. It can also be used to illustrate and elucidate universal features of the escape from a potential well, the jumps from one-well to cross-well motions displaying similar characteristics to those recently charted for the cubic one-well potential. We identify here some new codimension-two global bifurcations which serve to organize the bifurcation set and structure the related basin explosions and escape phenomena.

1. Introduction

Many new and exotic phenomena are being discovered and elucidated in the current renaissance of nonlinear dissipative dynamics (Abraham & Shaw 1982–8; Guckenheimer & Holmes 1983; Thompson & Stewart, 1986; Moon 1987). In particular, the unexpected chaotic behaviour of deterministic systems (Lorenz 1963; Ueda 1973, 1978) has provoked great interest among physical scientists, blurring the previous sharp distinctions between deterministic and stochastic views of the world. This unexpected behaviour embraces both the steady chaotic motions on chaotic attractors, and the transient chaos that can occur even in situations where all the final attractors are regular and periodic. One important consequence of these chaotic transients is that the basin boundaries between competing, coexisting steady states can have an infinitely tangled homoclinic structure (Hayashi *et al.* 1970), whose fractal properties have recently been the object of much study (McDonald *et al.* 1985; Moon & Li 1985; Eschenazi *et al.* 1989; Thompson & Soliman 1990). Here, even though any trajectory over a finite time interval depends continuously on the initial conditions, the dependence can be extremely sensitive; so when final behaviour is considered in the limit as the time tends to infinity, the attractor ultimately chosen may depend discontinuously on the initial conditions in a substantial region of phase space corresponding to the fractal basin boundary. From this point of view, long-term predictability is lost.

Chaotic attractors, their bifurcations, and fractal basin boundaries have recently been shown to play a key role in the escape of periodically driven oscillators from a

Phil. Trans. R. Soc. Lond. A (1990), **332**, 169–186 *Printed in Great Britain*

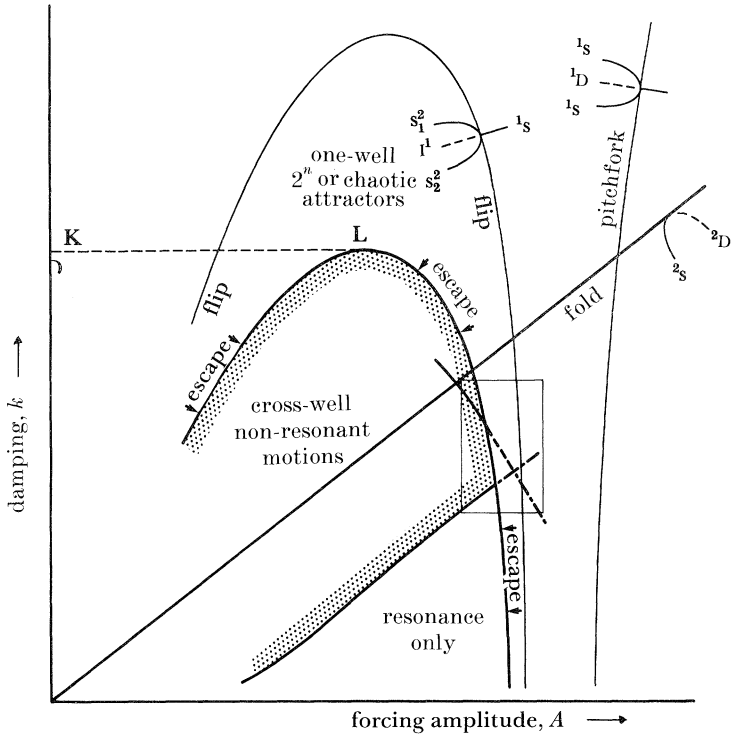

Figure 1. A sketch of the major bifurcation arcs in the (k, A) parameter space: the rectangle shows the region of the current investigation.

potential well, a problem of very wide interest to chemists, physicists and engineers (Thompson 1989). The present work examines the twin-well forced Duffing oscillator, and shows that as a control parameter is slowly varied there can arise abrupt and discontinuous changes in the fractal boundaries (fractal–fractal basin bifurcations or basin explosions), which are closely related to the escape from one-well to cross-well motions. The basin bifurcations and escape curves are intimately interwoven with the more familiar phenomena of nonlinear dynamics (saddle-node fold bifurcations, period-doubling flip bifurcations, homoclinic tangencies, blue sky catastrophes, etc.) in a complex central region of control space. The exploration and clarification of this region, whose phenomena seem to have significant general relevance to the dynamics of driven nonlinear oscillators, is the major contribution of the present study.

2. Overview and some counter-intuitive escape routes

In our study of the twin-well Duffing oscillator we shall be holding the driving frequency constant: at a value which we shall see is $10^{\frac{1}{2}}/2$ (≈ 1.58) times the linear natural frequency of small undriven, undamped oscillations in one of the two wells. The driving amplitude A and the damping magnitude k are then the two control parameters of interest, and figure 1 gives a schematic overview of some of the major bifurcations in (A, k) space. The small rectangle shows the domain of our main investigation, $0.3 < A < 0.36$, $0.14 < k < 0.24$, which is blown-up into figure 9, but before proceeding it is of interest to examine some of the overall escape features.

Escape from single-well to cross-well motions will occur on crossing the indicated

bifurcation arc, which means that escape can easily be triggered, counter-intuitively, by a decrease in the forcing magnitude, A. Escape is clearly achieved most simply from zero forcing amplitude, by gradually increasing A, at fixed damping $k < K$, along a horizontal path below the segment KL. However, starting again from zero forcing with damping greater than K, the forcing amplitude may be increased gradually from zero without causing escape (in the sense that we shall explain later in terms of the dynamic hilltop ^{1}D). By following a path above segment KL to the right of L, then decreasing damping below the level of KL, it is then possible to trigger escape by a subsequent decrease in the forcing amplitude. (It should be noted that further attractors not described here may coexist with the one-well or cross-well attractors whose régimes are indicated in this figure; but these additional attractors are not observed in the scenarios just described.)

Similar counter-intuitive behaviour can also be seen in Thompson (1989, fig. 3) for the escape from his cubic single-well. On this figure we could first increase the forcing magnitude F from zero at a sufficiently high frequency (above ω^R) until the response is close to a fold (line GG): we could then reduce the forcing frequency at constant F to arrive above a Feigenbaum cascade: a final reduction in F would lead to period-doubling, chaos and escape along the route gfF of Thompson (1989, fig. 4*a*).

3. System definition and attractor bifurcations

We consider Duffing's equation,

$$\ddot{x} + k\dot{x} + \alpha x + x^3 = A \sin t, \tag{1}$$

which we can write as two first-order equations,

$$\dot{x} = y, \quad \dot{y} = -ky - \alpha x - x^3 + A \sin t, \tag{2}$$

with a dot denoting differentiation with respect to the time, t. Equation (2) can of course be conveniently converted to three autonomous equations of a ring model by replacing t by θ and adding the extra dummy equation $\dot{\theta} = 1$ with $0 \leqslant \theta < 2\pi$. We shall in fact hold α constant at -0.2 throughout the paper. This equation describes the motions of a forced oscillator with a nonlinear stiffness function, and is one of the most simple and representative nonlinear systems (Guckenheimer & Holmes 1983; Moon 1987): it represents, for example, the lateral vibrations of an elastic column compressed by an axial force in excess of the critical Euler buckling load. In equation (1) the parameter α is the linear restoring stiffness, and with α negative we have a twin-well potential given by

$$V(x) = \tfrac{1}{2}\alpha x^2 + \tfrac{1}{4}x^4 \quad (\alpha < 0). \tag{3}$$

With no forcing, $A = 0$, there exist two stable equilibrium states at $x = \pm(-\alpha)^{\frac{1}{2}}$. The linear natural (undamped) frequency of these free vibrations, ω_n, is given by the square root of the stiffness, $\alpha + 3x^2$, evaluated at either of the two equilibrium states: hence $\omega_n = 2/10^{\frac{1}{2}}$, and the ratio of the driving frequency ($\omega_f = 1$) to this linear frequency is $10^{\frac{1}{2}}/2 \approx 1.58$. With a small intensity of sinusoidal forcing, these two point attractors become harmonic periodic attractors in the two wells, the one realized in a given time integration depending of course on the starting conditions of the motion. Notice that we use the adjective harmonic to mean isochronous, describing motions that have the same period as the driving function. These steady state solutions within a single well are called one-well motions. As we slowly vary the

parameters, making A large for example, a one-well motion will sometimes escape from its well to become a cross-well motion. The one-well and cross-well attractors can be either periodic or chaotic, depending on the system parameters (Ueda *et al.* 1987).

The periodically forced second-order oscillator (1) requires three coordinates, (x, y, t) to uniquely specify an initial condition for a continuous trajectory. However, by the device of taking a Poincaré section, we may reduce the problem to a phase space of dimension two, provided that we implicitly substitute a Poincaré map, or diffeomorphism, for the original flow (Guckenheimer & Holmes 1983; Thompson & Stewart 1986). Throughout this paper we use the Poincaré section obtained by sampling trajectories of (1) stroboscopically at $t = 2\pi n$ ($n = 0, 1, 2, \ldots$). As a result of this sampling, periodic solutions of (1) become fixed points or periodic points in the Poincaré section.

Bifurcations of the attractors relevant to the escape process are shown in the three diagrams of figure 2 for three values of the damping parameter k, the steady-state stroboscopically sampled x and y being plotted against the forcing amplitude A. The computations for these diagrams used single precision, fourth-order Runge–Kutta numerical integrations with time step $2\pi/60$: for every new value of A a few hundred forcing cycles were discarded to eliminate transients, and the representative steady-state points were projected onto the x and y axes. Such bifurcation diagrams indicate how the dynamical behaviour would evolve in a physical system in which the forcing amplitude is varied in a slow quasi-static manner. In each diagram there exists at the largest value of A two one-well motions (one in each well) and one resonant cross-well motion, the one-well motions having already started a period-doubling cascade in the case of figure 2*c*. Notice that we reserve the adjective resonant for the large amplitude cross-well harmonic motions of period 2π. Under decreasing A, the cross-well resonant motion is essentially unchanged, but the two complementary one-well motions exhibit a cascade of period-doubling flip bifurcations leading to a one-well chaotic attractor, and when A reaches A_{esc} the one-well motions escape out of their respective wells. However, in figure 2*a* and *c* the escape is to a chaotic cross-well motion, while in figure *b* escape involves a jump to the large amplitude resonant state. Moreover, for the case in figure *c* the cross-well chaotic attractor after escape undergoes a subsequent discontinuous enlargement or explosion at A_{ff}. A classic study of attractor explosion is that of Ueda (1980).

The goal of the present paper is to elucidate and explain these three escape scenarios, and to do this we must look, not only at the attractors and their bifurcations, but also at the basin boundaries and their bifurcations. In doing this, we shall throughout focus particular attention on bifurcations which are discontinuous in the sense of Zeeman (1982) with the locus in phase space of an attracting set and a basin, or both, changing discontinuously as a function of some parameter.

4. Basin boundary bifurcations

Before presenting our studies of basin bifurcations (what Grebogi *et al.* (1987) call basin boundary metamorphoses), we must here explain our notation for the fixed points. We use the symbol S for a stable attracting solution (a sink), D for a directly unstable saddle with positive mapping eigenvalues, and I for an inversely unstable saddle with negative eigenvalues: notice that our restriction to a positive linear damping coefficient, k, eliminates the possibility of an unstable repellor (a source), U,

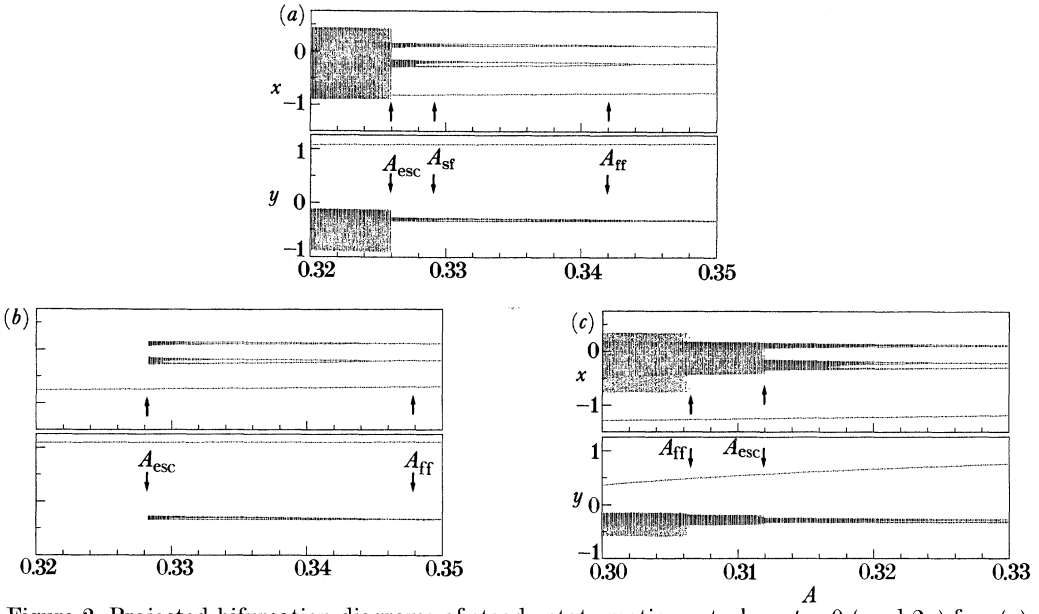

Figure 2. Projected bifurcation diagrams of steady-state motions at phase $t = 0$ (mod 2π) for: (*a*) $k = 0.164$, $A = 0.32$–0.35; (*b*) $k = 0.150$, $A = 0.32$–0.35; (*c*) $k = 0.230$, $A = 0.30$–0.33. In each diagram A is decreased from three distinct starting conditions at the right-hand edge corresponding to the two one-well motions and the single harmonic resonant cross-well motion: in (*c*) the one-well motions have already begun their period-doubling cascade at the starting value of A.

due to constraints on the mapping eigenvalues (see, for example, Thompson, 1989). These symbols carry suffices, i, j, l, in the manner of ${}^{l}\mathrm{S}^{i}_{j}$, with i indicating the order of the periodic point ($i = 1$ for a harmonic motion of period 2π, $i = 2$ for a subharmonic motion of period 4π, etc.), j indicting the sequence of movement from one point to the next (so that $l \leqslant j \leqslant i$), and l representing the group of periodic points (a different number l being assigned arbitrarily to each individual solution as a distinguishing code). Suffices are however sometimes omitted, for simplicity, in cases in which no confusion is possible. The symmetry of equation (2), associated with its invariance under the transformation $x \to -x, y \to -y, t \to t+\pi$, implies that one-well solutions always come in pairs, one for each well; such pairs are given identical symbols, but are distinguished by adding a prime to the solution in the right-hand well. Finally, in the attractor–basin phase portraits, a solid black circular dot is used to denote an unstable D solution; a hollow circular dot indicates a sink (S); while a solid square dot indicates an unstable I solution.

4.1. *Representative attractor–basin phase portraits*

To summarize the phenomena under consideration, we show first in figure 3 examples of the attractor–basin phase portraits containing two symmetrically-related one-well harmonic attractors, ${}^{1}\mathrm{S}$ and ${}^{1}\mathrm{S}'$ together with the resonant cross-well harmonic attractor, ${}^{2}\mathrm{S}$. These three attractors are all 2π periodic motions, and are represented by the three open circles in figure 3*a*. Notice that ${}^{1}\mathrm{S}$ and ${}^{1}\mathrm{S}'$ do not appear to be symmetric in this figure because both are sampled stroboscopically at the same phase $t = 0$ (mod 2π); their symmetry would only be apparent if one of the two were sampled at $t = \pi$ (mod 2π). The shaded region in figure 3*a* shows the basin of attraction of the resonant cross-well attractor, while the blank region represents the

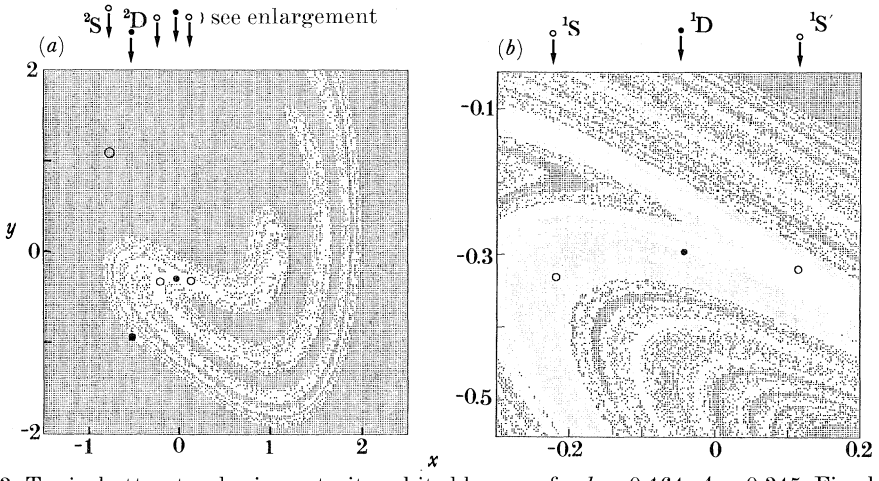

Figure 3. Typical attractor–basin portrait and its blow-up, for $k = 0.164$, $A = 0.345$. Fixed points shown are: ^{1}D, $(-0.0429, -0.2966)$; ^{1}S, $(-0.2187, -0.3315)$; ^{1}S′, $(0.1142, -0.3203)$; ^{2}D, $(-0.5309, -0.9492)$; ^{2}S, $(-0.7785, 1.0949)$. In the portrait (*a*), dark grey denotes the basin of the cross-well attractor ^{2}S, white denotes the union of the basins of ^{1}S and ^{1}S′. In the enlargement (*b*), dark grey denotes the basin of the cross-well attractor ^{2}S, light grey denotes the basin of the one-well attractor ^{1}S, white denotes the basin of the one-well attractor ^{1}S′.

union of the basins of the one-well attractors, the fractal boundary of the resonant cross-well basin being defined by the inset of the saddle solution ^{2}D. In computing figure 3, and all attractor–basin portraits in this paper, a fourth-order Runge–Kutta difference scheme with fixed step size equal to $2\pi/60$ was used with double precision: initial conditions were chosen on a uniform grid of 201×201 points, integrations being continued for about 100 forcing cycles from each grid point.

Note that for brevity we shall hereafter describe all states other than the harmonic cross-well resonant motion as non-resonant whether they be cross-well or one-well motions: in particular, any one-well or cross-well motions that are not 2π periodic are designated as non-resonant.

Figure 3*b* is a magnified blow-up of the non-resonant attractor basin, showing the two one-well attractors ^{1}S and ^{1}S′ and their individual basins (distinguished by the white and light grey tone) separated by the inset of the hill-top saddle point ^{1}D. We refer to ^{1}D as the hill-top saddle because if we decrease the forcing amplitude to zero, ^{1}D evolves smoothly to the unstable equilibrium point at $x = y = 0$ which separates the two potential wells. With non-zero forcing ^{1}D represents a dynamic barrier between potential wells. Some care is needed in formulating a precise definition of this dynamic barrier in operational terms. In cases where ^{1}D is not homoclinic, we may characterize the dynamic barrier in relatively straightforward fashion by the existence of a small neighbourhood of initial conditions around ^{1}D whose right half (demarcated by the inset or stable manifold of ^{1}D) end up in the right-hand well, while the left half settle to the left-hand well. However, in the parameter régime of particular interest in this study, ^{1}D is homoclinic, implying that either the basin boundary between the left and right one-well attractors has an infinitely fine fractal structure near ^{1}D, or else there are no one-well attractors, only cross-well attractors. In this case, the following more subtle characterization of the dynamic hilltop is appropriate: in a sufficiently small neighbourhood of ^{1}D, initial conditions in the left half (demarcated by the inwards eigenvector and its local continuation as the inset)

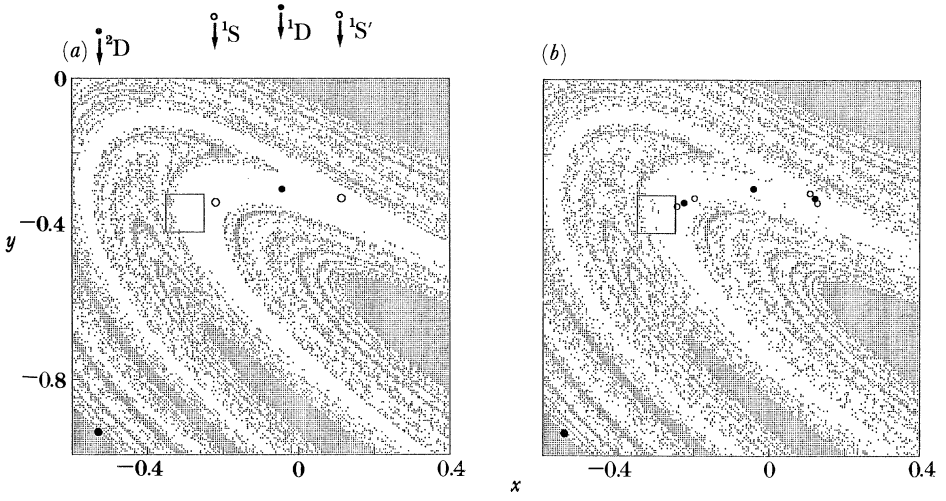

Figure 4. Attractor–basin phase portraits for two values of A straddling A_{ff} of figure 2a with: (a) $k = 0.164$, $A = 0.345$; (b) $k = 0.164$, $A = 0.340$.

always move to the left at the end of the first forcing cycle, while initial conditions in the right half move to the right at the end of the first forcing cycle. Indeed, we shall distinguish one-well motions from cross-well motions with reference to the dynamic hill-top ^{1}D and not with reference to the static hill-top $x = y = 0$.

We can see that in figure 3a, b the boundary separating the basin of ^{1}S from the basin of ^{1}S′ is tangled and has a fractal character. There do of course exist infinitely many higher-order unstable subharmonics in these phase portraits which are not shown here, but they exert no significant influence on the phenomena under discussion in the present paper.

4.2. *Fractal–fractal basin bifurcations*

Figure 4 shows the attractor-basin phase portraits for two values of A on either side of the critical value A_{ff} of figure 2a. In progressing under decreasing A from figure 4a to 4b the one-well stable fixed points have experienced a period-doubling flip, but in both diagrams the union of the non-resonant basins is indicated by the white: motions starting in the shaded region terminate on the cross-well resonant motion. We see that in both diagrams of figure 4 the basin boundary has a fractal structure, but a closer inspection reveals significant differences which are shown in the blow-up of the framed regions in figure 5. In figure 5a the resonant region is limited by the inset of the $i = 3$ periodic point ^{2}D^3 which prevents the tails of the resonant attracting region passing to the right of ^{2}D^3. However, in figure 5b it is the inset of the $i = 3$ periodic point ^{1}D^3 which limits the penetration of the resonant attracting region. This change in what Grebogi *et al.* (1987) term the accessible orbit occurs discontinuously at the parameter value A_{ff} and is called a fractal–fractal basin bifurcation (or metamorphosis). For $k = 0.164$ we have established that A_{ff} lies in the interval 0.3418–0.3420.

Note here that in figure 5 the $i = 3$ periodic points, ^{1}D^3 and ^{1}I^3 have been created by a fold-flip scenario similar to that illustrated for an $i = 6$ periodic motion by Thompson (1989) in his figure 9 (using data supplied by Y. Ueda). Under decreasing A, a fold at $A \approx 0.3497$ first creates a saddle-node pair, ^{1}D^3 and ^{1}S^3 (and the

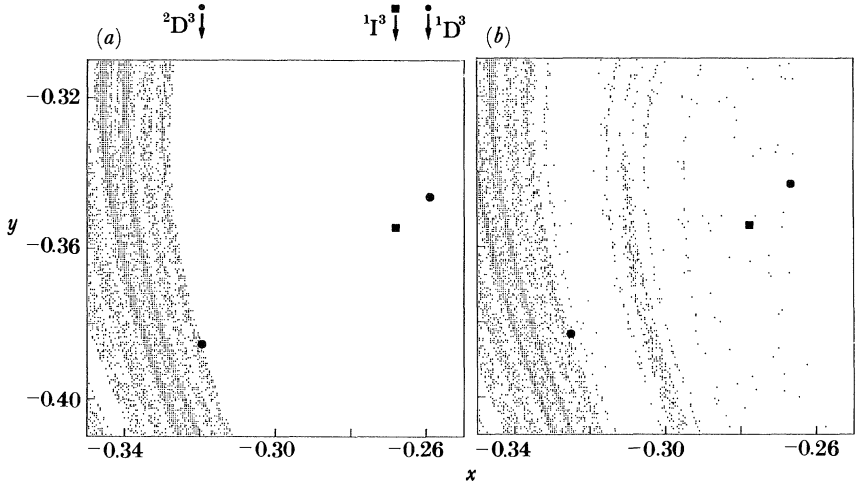

Figure 5. Enlargements of the small frames of figure 4, showing attractor–basin features above and below A_{ff} of figure 2*a*. In the portrait (*a*), $k = 0.164$, $A = 0.345$, with fixed points: $^1D^3$, $(-0.2590, -0.3463)$; $^1I^3$, $(-0.2682, -0.3545)$; $^2D^3$, $(-0.3194, -0.3855)$. In the portrait (*b*), $k = 0.164$, $A = 0.340$, with fixed points: $^1D^3$, $(-0.2666, -0.3434)$; $^1I^3$, $(-0.2776, -0.3544)$; $^2D^3$, $(-0.3251, -0.3833)$.

corresponding $^1D^{3\prime}$ and $^1S^{3\prime}$) inside the basin of the one-well attractor. The stable solution, $^1S^3$, then experiences a period-doubling bifurcation at $A \approx 0.3482$ generating $^1I^3$, followed rapidly by a complete cascade to a chaotic attractor which finally vanishes at a blue-sky catastrophe. This fold–flip–cascade–crisis scenario occupies an extremely small parameter range, and the corresponding basins of attraction are restricted to very small areas of phase space: indeed the aspects of this scenario can only just be resolved by very precise numerical investigations.

The fold and flip in this scenario are precisely those described by Gavrilov & Shilnikov (1972, 1973), who prove that similar events are expected for periodic points of all orders. However, in our experience, the primary observable effect of these complex bifurcations, namely the appearance of attractors, is extremely slight for low-order periodic points, and virtually nil for higher periodic points. Indeed, our main concern here is not with $^1S^3$ or $^1I^3$, but with $^1D^3$ and its role in defining the basin of the resonant motion.

4.3. *Smooth-fractal basin bifurcations*

Figure 6 shows the attractor-basin phase portraits for two values of A just above and below the critical value of A_{sf} marked in figure 2*a*. Here, with $k = 0.164$, A_{sf} lies in the range 0.3291–0.3292, and at A_{sf} the fractal structure of the basin boundary disappears instantaneously. Moreover, with decreasing A a cascade of flip bifurcations transforms the two one-well periodic attractors into chaotic attractors. Each of these chaotic attractors, visible in figure 6*b*, is a simply folded band, containing the inversely unstable fixed point ^1I (or $^1I'$), whose outstructures intersect in a dollar-sign pattern (see Rössler 1976, 1979).

We have also made during the course of this investigation a white and light-grey study to observe, in addition, the boundary between the two one-well chaotic attractors. This diagram, not reproduced here, shows clearly that the inner boundary is still fractal although the outer boundary is now smooth.

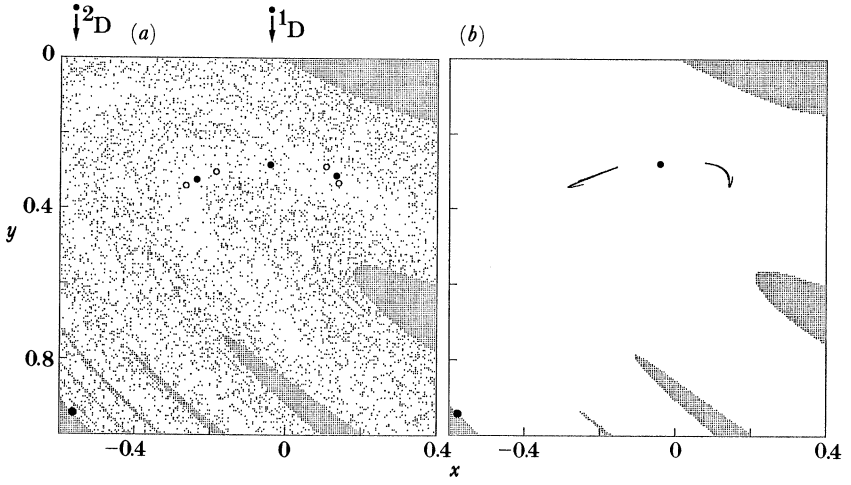

Figure 6. Attractor–basin phase portraits for two values of A straddling A_{sf} of figure 2a. In the diagram (a), $k = 0.164$, $A = 0.332$; in the diagram (b), $k = 0.164$, $A = 0.327$.

The sudden and dramatic penetration of the bulk of the white basin during the small parameter change from figure 6b–a could have severe consequences for the integrity of an operating engineering system: it is an example of the type of basin erosion highlighted recently by Soliman & Thompson (1989).

5. The invariant manifolds and their tangencies

To understand the mechanisms governing these various phenomena, we now look more closely at the invariant manifolds of the saddle cycles. We adopt the neat terminology introduced by Christopher Zeeman, referring to a stable manifold as an inset, an unstable manifold as an outset, and we call the totality of the invariant manifolds the outstructures, following Abraham (1985).

5.1. *Saddle outstructures and the basin bifurcations*

The recent studies of Grebogi *et al.* (1987) have shown that a basin boundary bifurcation (metamorphosis) of the Hénon map is governed by a homoclinic tangency of the inset and the outset of a saddle. Here we identify a similar situation in the discrete Poincaré mapping derived by stroboscopic sampling of our forced Duffing oscillator, when we investigate the mechanisms underlying figure 2.

The schematic diagrams of figure 7 are sketches of the outstructures of the hill-top saddle ^{1}D and the $i = 3$ periodic point ^{2}D^3, corresponding to the fractal-fractal metamorphosis of figures 4 and 5. These are based on detailed numerical constructions of the outstructures; however, because some features are difficult to see in the original computer-generated plots, we have drawn schematic diagrams for clarity. Insets and outsets can be distinguished by the arrows. In figure 7a the branch of the outset of ^{2}D^3 which tends towards the non-resonant attractors (indicated by double arrows) is close to, but does not cross, the inset of ^{2}D^3, and so does not form a homoclinic cycle (the other outset does). Any orbit starting on the side of the inset of ^{2}D^3 which faces the non-resonant attractors can never reach the other side of the inset of ^{2}D^3, and so can never reach the resonant attractor. The inset

of $^2D^3$ thus acts as a barrier shutting out the tails of the resonant attractive domain, and constitutes the basin boundary for the non-resonant attractors. But remember that the resonant attractor ^2S has a fractal basin, and outside the insets of $^2D^3$ there are accumulated the infinitely narrow fractal tails of the resonant basin. This is because the branch of the outset of $^2D^3$ directed away from the non-resonant attractors (indicated by single arrows) is homoclinic, so orbits started on that side of the inset of $^2D^3$ may eventually reach either the resonant attractor or the non-resonant attractors. (Indeed, this outward branch of the outset of $^2D^3$ transversely intersects the inset of ^2D, and the outset of ^2D intersects the inset of $^2D^3$; i.e. there is a Smale cycle involving ^2D and $^2D^3$.) We should emphasize that in figure 7*a*, *b* the dotted region is not a basin of attraction, the dots serving simply to highlight the position of the relevant inset.

In figure 7*b* the branch of the outset of $^2D^3$ tending toward the non-resonant attractors (indicated by double arrows) has now moved to intersect the inset of $^2D^3$, creating homoclinic cycles. As a consequence, the inset of $^2D^3$ no longer forms a barrier to the incursion of the narrow resonant tails: this role is taken by the inset of $^1D^3$, which has already appeared. In the terminology of Grebogi *et al.* $^1D^3$ is now the new accessible orbit. So we see that in this case the fractal–fractal basin bifurcation coincides with a homoclinic tangency of the inset and the outset of $^2D^3$ at A_{ff}.

As a note of explanation, it is perhaps worth emphasizing here that no trajectory can ever 'climb the wall' represented by an inset. However, when the inset becomes tangled, 'climbing the wall' should be understood in a local sense: although there are still two sides of the wall, the global structure of a tangled inset is often so complicated that a trajectory may superficially appear to end up on the other side.

In figure 7*c* we give a sketch of the outstructures of the $i = 3$ periodic point $^1D^3$ corresponding to the left-hand well, for the same parameter values as figure 7*b*. We note that the inward branch of the outset of $^1D^3$ is not homoclinic in figure 7*c*, just as the inward branch of the outset of $^2D^3$ was not homoclinic in figure 7*a*. For this reason, $^1D^3$ forms a barrier to the incursion of the narrow tails of the resonant attractor basin. This explains why in figure 5*b* we find no points of the basin of ^2S in the region lying roughly to the right of $^1D^3$, that is, on the inward side of the inset of $^1D^3$.

Finally, we observe that the inward branch of the outset of $^2D^3$ (indicated by double arrows) is always heteroclinic with the inset of ^1D, in figure 7*a*, *b*. For this reason, when $^2D^3$ becomes homoclinic, the tails of the resonant attractor basin become tangled with the (previously tangled) basins of ^1S and $^1S'$. That is, in figure 7*a* the basins of ^1S and $^1S'$ are tangled but adjacent and complementary, whereas in figure 7*b* we expect to find tails of the resonant attractor basin separating portions of the basins of ^1S and $^1S'$.

Turning now to the smooth-fractal basin bifurcation of figure 6, the relevant outstructures of the saddle point ^2D are sketched in figure 8. Figure 8*a* corresponds qualitatively to figure 5 of Grebogi *et al.* (1987), but the mapping within our tangle has a rather different structure. Most noticeably, our mapping contains the $i = 1$ unstable periodic point ^1D with positive multipliers inside the tangle, plus a pair of $i = 1$ unstable periodic points ^1I and $^1I'$ with negative multipliers; whereas their Hénon map tangle encloses only a single inversely unstable (I) $i = 1$ periodic point with negative multipliers, and no directly unstable (D) $i = 1$ periodic point. This difference of structure inside the tangle also corresponds to a different Birkhoff

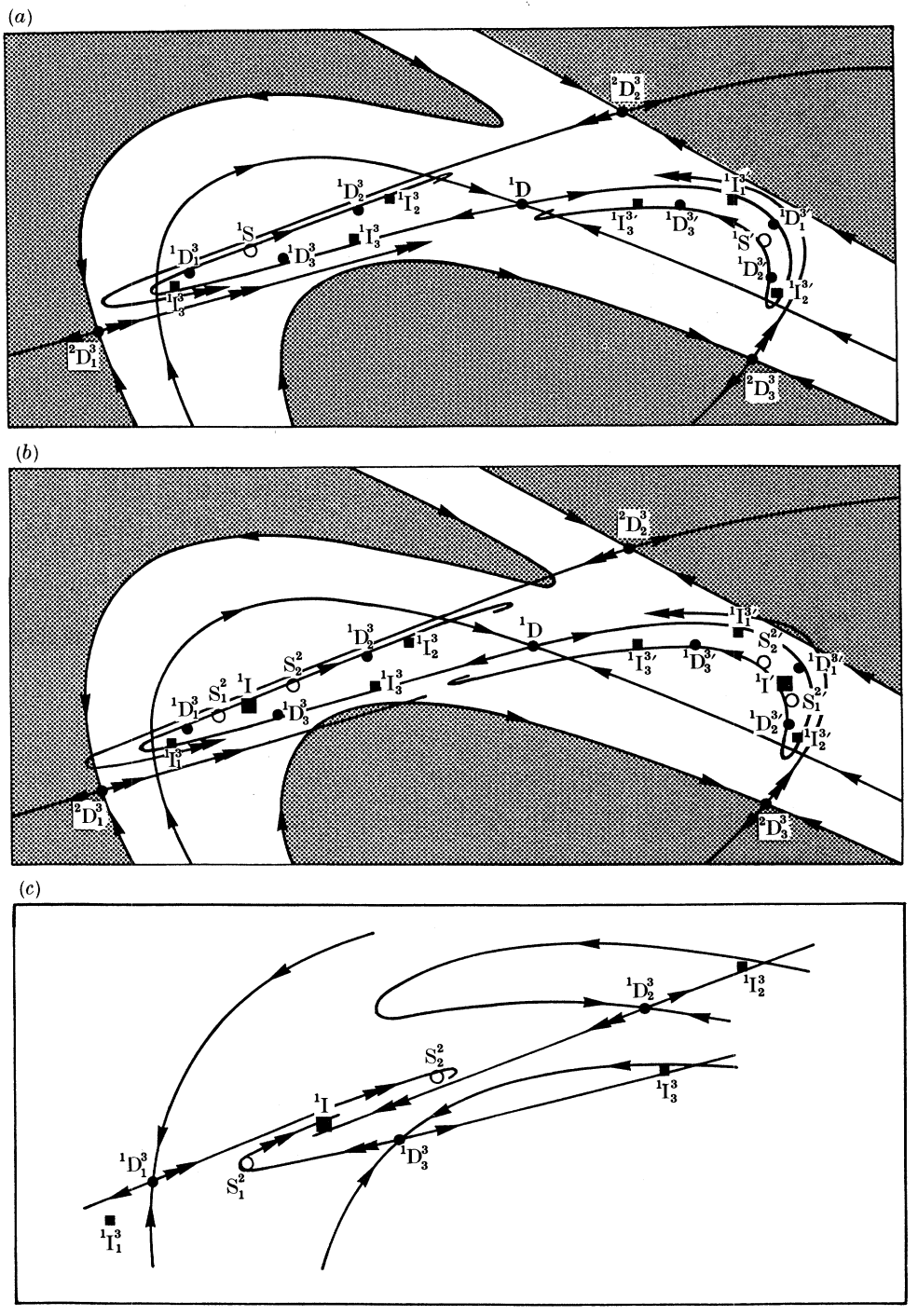

Figure 7. Schematic diagrams of the out structures (invariant manifolds) for the fractal–fractal basin bifurcation, with (*a*) and (*b*) corresponding to the diagrams of figure 4. Sketch (*c*) is a blow-up of the neighbourhood of the left-hand-well attractor. In (*a*) and (*b*) the dotted region is not a basin of attraction, the dots being used as a visual aid to highlight the position of the inset.

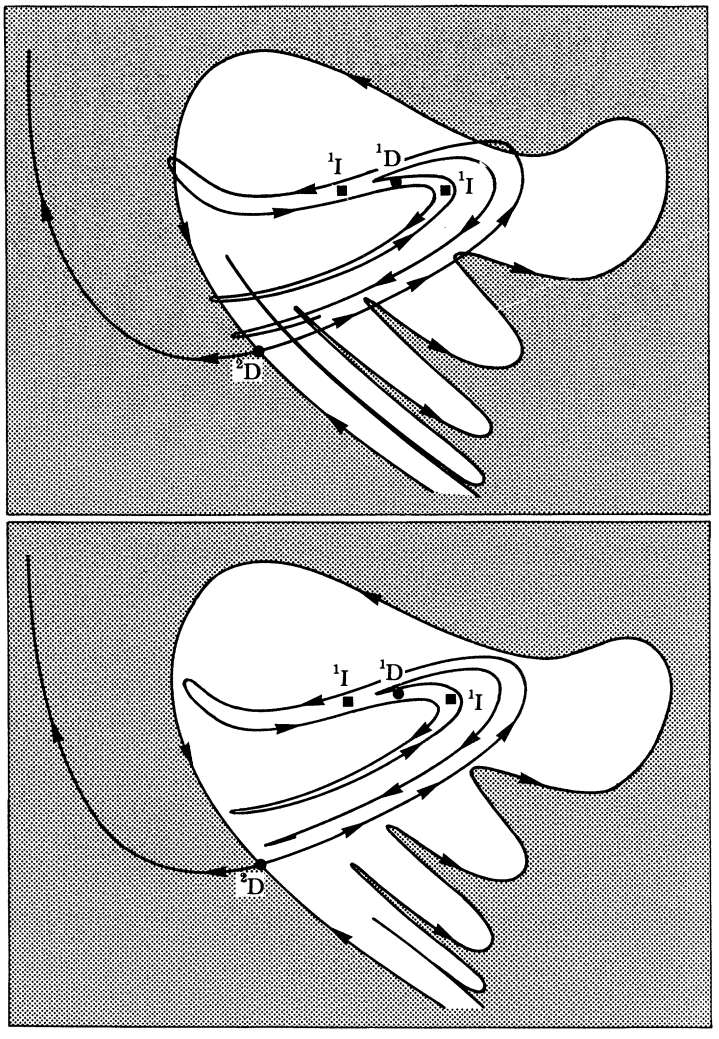

Figure 8. Schematic diagrams of the out structures (invariant manifolds) for the smooth-fractal basin bifurcation corresponding to A_{sf} of figure 2*a* and to figure 6*a*, *b*. The dot screen represents the resonant basin.

signature: in our case, when we number the points of homoclinic tangency consecutively, ..., H_{-2}, H_{-1}, H_0, H_1, H_2, ..., so that H_0 is adjacent to H_1, etc., we find that H_0 is mapped after one forcing cycle to H_2, while H_{-1} is mapped to H_1. So in our tangle the dynamics defines two distinct, interlaced sequences of homoclinic tangency points, whereas in the Hénon tangle there is only one sequence of tangency points.

5.2. *Codimension-two bifurcations of basins and attractors*

Having examined in detail the major basin bifurcations occurring in this region of parameter space, and the underlying structure of insets and outsets of the most important saddle points, we are prepared for a more comprehensive view of bifurcation patterns in parameter space. We continue to focus attention on the region of the (A, k) parameter space shown in figure 9. Here a number of important

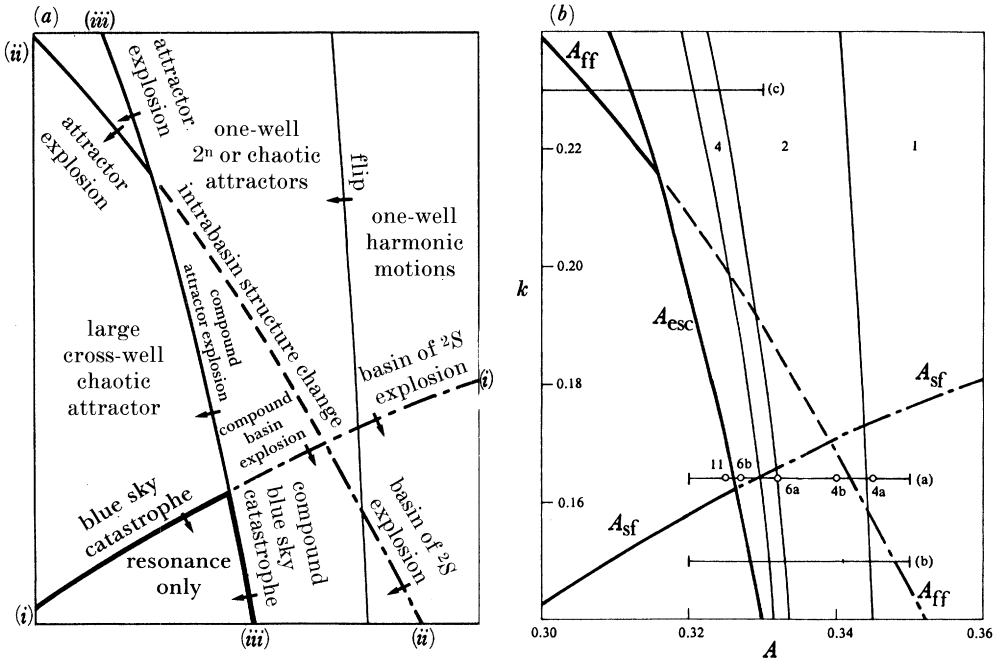

Figure 9. Two representations of the bifurcation arcs in the region of interest in the (A, k) parameter space. The three codimension-two events serve to organize the bifurcation set of figure 1. Homoclinic tangencies are (*i*) ^{2}D, (*ii*) ^{2}D^3, (*iii*) ^{1}D^3.

bifurcations come together in an intricate pattern that can be regarded as a backbone for the bifurcation set in a more extended régime, as seen in figure 1. Parameter values corresponding to the attractor-basin phase portraits of figures 4, 6 (and 11) are marked in figure 9*b* by small circles on the horizontal line (*a*). The lines (*a*), (*b*) and (*c*) in figure 9*b* show the paths of the attractor bifurcation diagrams of figure 2.

We can note first that the steady state 2π-periodic resonant motions exists throughout the whole domain of figure 9. Additionally, we have to the right of arc A_{esc} the non-resonant single well motions, there being no single-well motions to the left of this bifurcation arc. The fine arcs running roughly parallel to the escape arc are the low-order flip bifurcations corresponding to the start of the period-doubling cascade which converts the single-well motions, under decreasing A, into chaotic single-well attractors (cf. figure 6*b*) which then undergo catastrophic bifurcation at A_{esc}. The numerical values $(1, 2, 4)$ in the regions in figure 9*b* show the order of these one-well periodic attractors.

Apart from the arcs locating these flip bifurcations, there are three major bifurcation arcs indicated in figure 9*b*, labelled A_{esc}, A_{sf} and A_{ff}. Each of these arcs has an intrinsic definition as a homoclinical tangency of certain invariant manifolds. Thus the arc labelled A_{ff} is intrinsically defined as the locus in (A, k) space where ^{2}D^3 has a homoclinic tangency, involving the inward branch of the outset. Although this intrinsic definition of the arc applies over the full range of (A, k) values in figure 9, it will be noted that the effect of this global bifurcation on the attractor-basin portrait will differ depending on which segment of the arc is crossed. The intrinsic definitions and the attractor-basin descriptions are summarized in figure 9*a*; we shall now examine further the relations among these bifurcations.

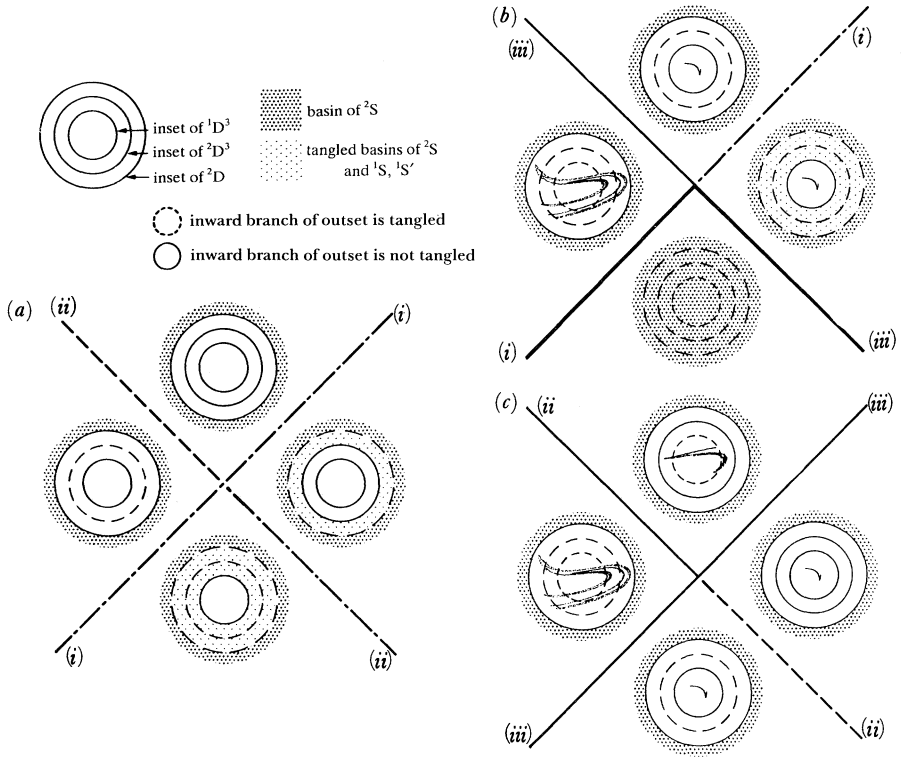

Figure 10. Schematic representations of the three codimension 2 events, showing attractor and basin explosions. Homoclinic tangencies are (*i*) ^{2}D, (*ii*) $^2D^3$, (*iii*) $^1D^3$.

For example, we have seen that crossing A_{ff} on the horizontal line (a) in figure 9*b*, there is an explosion in size of the basin of ^{2}S, at the expense of the basins of ^{1}S and ^{1}S′. The same is true crossing A_{ff} anywhere in the dot-dashed segment, below A_{sf}. But if A_{ff} is crossed above A_{sf}, in the dashed segment, there is no explosion in basin locus, even though $^2D^3$ still reaches homoclinic tangency.

These facts are summarized by figure 10*a*, in which simplified schematic diagrams suggest the relations of the insets of the key saddle points to the loci of basins of attraction (of course the representation of insets by circles is only a schematic device). For any uniformly dissipative dynamical system in euclidean phase space, insets and basins must always extend (backward in time) to infinity. We have chosen bounded representations for insets and basins in order to clarify the relative locations of the sets. It might be imagined, for example, that a transformation of phase space has been applied that brings the outer reaches of the phase space into a bounded region.

We note that the use of a circle to stand for an inset has a specific justification in cases where the inset is transversely homoclinic. The circle may then represent not the inset, but the maximal bounded invariant set associated with the tangle; that is, the ensemble of homoclinic points and related periodic points, the latter being dense in the invariant set. This bounded invariant set has a roughly annular shape, and may act as a separator if the underlying fixed point is of D type. The bounded invariant set of a tangled separator has been called a chaotic saddle (Stewart 1987).

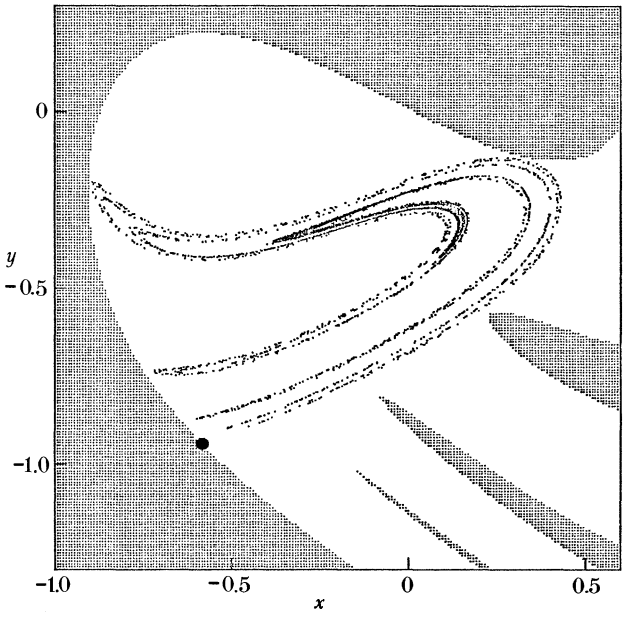

Figure 11. Attractor-basin phase portrait for $k = 0.164$, $A = 0.325$, showing the large cross-well chaotic attractor approaching a blue-sky collision with ^{2}D as k is reduced towards the bifurcation arc A_{sf}.

Beginning in the upper quadrant of figure 10*a*, we have a basin configuration similar to figure 6*b*, with the basin boundary of ^{2}S being smooth. Moving to the right quadrant, a homoclinic tangency of ^{2}D causes a first inward explosion of the basin of ^{2}S, similar to figure 4*a*. Proceeding to the lower quadrant causes a second inward basin explosion, similar to figure 4*b*. If instead we move from the upper quadrant of figure 10*a* to the left quadrant, no explosion is observed; only upon crossing to the lower quadrant do we find a chained or compounded basin explosion, which was prepared by the tangency of ^{2}D^3 but only realized by the tangency of ^{2}D. We believe that such a chained explosion pattern is a generic codimension-two global bifurcation of dissipative dynamical systems. In particular, any small change of a parameter other than (A, k), such as α, would simply alter the location of this codimension-two point in the (A, k) parameter space, leaving its qualitative features unchanged.

Note that the inward branch of the outset of ^{2}D is always transversely heteroclinic to the inset of ^{2}D^3 in this régime. So if the outset of ^{2}D^3 transversely intersects the inset of ^{2}D, then ^{2}D and ^{2}D^3 form a Smale cycle, and the inward branch of the outset of ^{2}D is necessarily homoclinic. In this régime, the converse is also true: if the inward branch of the outset of ^{2}D is transversely homoclinic, then ^{2}D and ^{2}D^3 form a Smale cycle. (If this were not the case, we would find it necessary to take account of some other unstable point of D type, generating an additional, intermediate circle in our schematic diagram.) Likewise, the inward branch of the outset of ^{2}D^3 is homoclinic precisely when ^{1}D^3 and ^{2}D^3 form a Smale cycle. Figure 10*a* should be read keeping in mind that the dashed circle stands both for the inward homoclinic intersection and for a Smale cycle with the saddle in the next circle inward.

Another codimension-two bifurcation apparent in figure 9 lies at the intersection of A_{esc} (homoclinic tangency of ^{1}D^3) with A_{sf} (homoclinic tangency of ^{2}D). Here three

of the four bifurcations involve attractors, so it may be helpful to refer again to figure 2.

Crossing A_{esc} at $k = 0.150$ as in figure 2*b*, we see that the one-well chaotic attractors suffer a blue sky catastrophe at $A = A_{esc}$, transients from either of the formerly stable chaotic attractors lead to the resonant cross-well periodic attractor. At the bifurcation threshold, the one-well chaotic attractors just touch the saddle points $^1D^3$ and $^1D^{3\prime}$ respectively. The one-well chaotic attractors do not touch the hilltop saddle ^1D at the bifurcation threshold; ^1D became transversely homoclinic prior to the attractor disappearance. Note that ^1D is the lowest-order unstable periodic orbit in the basin boundary of either one-well attractor; indeed we take an orbit crossing the inset of ^1D as our definition of escape. Since the fundamental saddle remains at a distance from the chaotic attractor when the catastrophic bifurcation occurs, this is a chaotic saddle catastrophe in the sense of Stewart (1987). This qualitative description holds whenever A crosses A_{esc} below A_{sf} in figure 9*b*.

Crossing A_{esc} above A_{sf} at $k = 0.164$ as in figure 2*a*, we again find the one-well chaotic attractors losing stability, this time via an attractor explosion to a large cross-well chaotic attractor, as illustrated in the phase portrait of figure 11. This cross-well chaotic attractor is numerically identical with the closure of the outset of $^2D^3$ (it contains the outsets of $^1D^3$ and ^1D as well). Note that in figure 11, ^2D is near homoclinic tangency; if we hold $A = 0.325$ and decrease k from 0.164 so that A_{sf} is crossed to the left of A_{esc}, the homoclinic tangency of ^2D causes a blue sky catastrophe for the large cross-well chaotic attractor. This is a regular saddle catastrophe; the fundamental saddle in the basin boundary is ^2D, which reaches homoclinic tangency precisely as the blue sky catastrophe occurs. Equivalently, the basin boundary approaches a loss of regularity at the blue sky catastrophe threshold.

These events are summarized in figure 10*b*, using schematic diagrams similar to figure 10*a*. Here solid curves represent attractor bifurcations; the thinner arc is explosive, while the thicker arcs stand for blue sky catastrophe. The dot–dashed segment, as in figure 10*a*, stands for an explosion in locus of a basin. This fourth leg of the codimension two bifurcation can be seen as preparation for a chained or compounded bifurcation, combining the attractor explosion with the blue-sky catastrophe, which occurred as distinct events on the left side of figure 10*b*. The chaining is prepared by completing a heteroclinic connection from the outward branch of the outset of $^1D^3$ to the inset of $^2D^3$ and thence via the outward outset of $^2D^3$ to the inset of ^2D.

A third generic type of codimension two event occurs near the top of figure 9 where the bifurcation arcs labelled A_{ff} (homoclinic tangency of $^2D^3$) and A_{esc} (homoclinic tangency of $^1D^3$) intersect. As shown in figure 2*c*, there are two distinct chaotic attractor explosions above this codimension two point. Crossing A_{esc} the one-well chaotic attractors explode to a single cross-well attractor. This chaotic attractor is intermediate in size, since it contains the unstable points $^1D^3$ and $^1D^{3\prime}$ and their outsets, but does not contain the unstable motion $^2D^3$. This intermediate size cross-well chaotic attractor subsequently explodes to a larger chaotic attractor when A_{ff} is crossed; the larger attractor does contain $^2D^3$ and its outset, and is essentially the same as the attractor shown in figure 11.

Starting again from the smaller one-well chaotic attractors to the right of A_{esc} and below the codimension two intersection with A_{ff}, we find that crossing A_{ff} now has no effect on attractor size, whereas crossing A_{esc} results in a chained or compound attractor explosion. This situation is schematized in figure 10*c*. Here the dashed

segment of bifurcation arc can be seen as a preparation for the compound explosion: when the inward branch of the outset of $^2D^3$ becomes homoclinic, the outward branches of the outsets of $^1D^3$ and $^1D^{3\prime}$ simultaneously form a heteroclinic connection to the inset of $^2D^3$. Thus $^1D^3$ and $^1D^{3\prime}$ are chained to $^2D^3$, and the subsequent attractor explosion will bring $^2D^3$ as well as $^1D^3$ and $^1D^{3\prime}$ inside the chaotic attractor.

Note that in this case, the preparatory bifurcation causes neither a discontinuous change in attractor nor in basins, but only a discontinuous change in part of the non-wandering set in the interior of a basin. This change in the non-wandering set effects only the structure of transients in the basin. As in figures 9 and 10*a*, this most subtle type of global bifurcation is indicated by a dashed segment of arc.

In short we have identified three distinct types of codimension-two global bifurcation in the régime of figure 9. Each is an apparently generic pattern in which two distinct discontinuous bifurcations in the attractor-basin phase portrait become chained to produce a compound event. A preparatory bifurcation is required in each codimension two pattern. For the compound blue sky catastrophe, the preparation causes a basin explosion; but for the compound attractor explosion as well as for the compound basin explosion, the preparation is a subtle global bifurcation which has no discontinuous effect on the loci of either attractors or basins. The three types of codimension two bifurcation dovetail neatly together, organizing the bifurcation arcs in the regime under study. The codimension-one bifurcations extend to a much wider range of parameter values, so that the régime under study, although rather small, is central to the overall behaviour of equation (1).

6. Conclusions

We have studied the occurrence of basin boundary bifurcations in the forced twin-well Duffing oscillator, as well as global bifurcations of chaotic attractors which lead to escape from single-well to cross-well motions. We observed that in the régime considered, escape always occurs as a result of decreasing the forcing amplitude. Upon considering the underlying invariant manifold structures of the low order unstable points (harmonic and subharmonic of order 3), we found that the escape bifurcations and the abrupt, discontinuous basin bifurcations are intimately related, forming three distinct types of codimension two global bifurcations. These codimension two patterns appear to be generic for dissipative two-dimensional diffeomorphisms. At these codimension two points in the (A, k) parameter space, it becomes clear that the codimension one global bifurcations are only fully characterized when both their intrinsic definition as tangencies of invariant manifolds, and their attractor-basin phase portrait consequences are considered together. Similar phenomena can be expected to occur in the response of many driven nonlinear oscillators.

Y.U. and S.Y. would like to acknowledge use of the facilities at the Computer Centre of the Institute of Plasma Physics, Nagoya University, J.M.T.T. acknowledges with thanks the award of a Senior Fellowship by the Science & Engineering Research Council of Great Britain. H.B.S. acknowledges support from the Applied Mathematical Sciences Programme of the U.S. Department of Energy.

PHILOSOPHICAL TRANSACTIONS OF THE ROYAL SOCIETY A MATHEMATICAL, PHYSICAL & ENGINEERING SCIENCES

References

Abraham, R. H. 1985 Outstructures of the Lorenz attractor. In *Chaos, fractals and dynamics* (ed. P. Fischer & W. R. Smith). New York: Dekker.

Abraham, R. H. & Shaw, C. D. 1982–8 *Dynamics: The geometry of behaviour*: part 1, *Periodic behaviour* (1982); part 2, *Chaotic behaviour* (1983); part 3, *Global behaviour* (1985); part 4, *Bifurcation behaviour* (1988). Santa Cruz: Aerial Press.

Eschenazi, E., Solari, H. G. & Gilmore, R. 1989 Basins of attraction in driven dynamical systems. *Phys. Rev.* A **39**, 2609–2627.

Gavrilov, N. K. & Shilnikov, L. P. 1972–3 On three-dimensional dynamical systems close to systems with a structurally unstable homoclinic curve. *Math. USSR Sb.* **88**, 467–485; **90**, 139–156.

Grebogi, C., Ott, E. & Yorke, J. A. 1987 Basin boundary metamorphoses: changes in accessible boundary orbits. *Physica* D **24**, 243–262.

Guckenheimer, J. & Holmes, P. 1983 *Nonlinear oscillations, dynamical systems, and bifurcations of vector fields*. New York: Springer-Verlag.

Hayashi, C., Ueda, Y., Akamatsu, N. & Itakura, H. 1970 On the behaviour of self-oscillatory systems with external forcing. *Electron. Commun Jap.* A **53**, 31–39.

Lorenz, E. N. 1963 Deterministic nonperiodic flow. *J. atmos. Sci.* **20**, 130–141.

McDonald, S. W., Grebogi, C., Ott, E. & Yorke, J. A. 1985 Fractal basin boundaries. *Physica* D **17**, 125–153.

Moon, F. C. 1987 *Chaotic vibrations: An introduction for applied scientists and engineers*. New York: Wiley.

Moon, F. C. & Li, G. X. 1985 Fractal basin boundaries and homoclinic orbits for periodic motions in a two-well potential. *Phys. Rev. Lett.* **55**, 1439–1442.

Rössler, O. E. 1976 An equation for continuous chaos. *Physics Lett.* A **57**, 397–398.

Rössler, O. E. 1979 Chaos. In *Structural stability in physics* (ed. W. Guttinger & H. Eikemeier). Berlin: Springer.

Stewart, H. B. 1987 A chaotic saddle catastrophe in forced oscillators. In *Dynamical systems approaches to nonlinear problems in systems and circuits* (ed. F. Salam & M. Levi). Philadelphia: SIAM.

Soliman, M. S. & Thompson, J. M. T. 1989 Integrity measures quantifying the erosion of smooth and fractal basins of attraction. *J. Sound Vib.* **135**, 453–475.

Thompson, J. M. T. 1989 Chaotic phenomena triggering the escape from a potential well. *Proc. R. Soc. Lond.* A **421**, 195–225.

Thompson, J. M. T. & Soliman, M. S. 1990 Fractal control boundaries of driven oscillators and their relevance to safe engineering design. *Proc. R. Soc. Lond.* A **428**, 4–13.

Thompson, J. M. T. & Stewart, H. B. 1986 *Nonlinear dynamics and chaos*. Chichester: Wiley.

Ueda, Y. 1973 Computer simulation of nonlinear ordinary differential equations and nonperiodic oscillations. *Trans. Japan Inst. electr. Commun. Engrs* A **56**, 218–225.

Ueda, Y. 1978 Random phenomena resulting from nonlinearity – in the system described by Duffing's equation. *Trans. Japan Inst. Electr. Engrs* A **98**, 167–173.

Ueda, Y. 1980 Explosion of strange attractors exhibited by Duffing's equation. *Ann. N.Y. Acad. Sci.* **357**, 422–434.

Ueda, Y., Nakajima, H., Hikihara, T. & Stewart, H. B. 1987 Forced two-well potential Duffing's oscillator. In *Dynamical systems approaches to nonlinear problems in systems and circuits* (ed. F. Salam & M. Levi). Philadelphia: SIAM.

Zeeman, E. C. 1982 Bifurcation and catastrophe theory. In *Papers in algebra, analysis, and statistics* (ed. R. Lidl), pp. 207–272. Providence: American Mathematical Society.

PHILOSOPHICAL TRANSACTIONS OF THE ROYAL SOCIETY A MATHEMATICAL, PHYSICAL & ENGINEERING SCIENCES